



SEISMIC PERFORMANCE OF A STRUCTURAL WALL BUILDING WITH GEOMETRIC AND REINFORCEMENT DISCONTINUITIES

J. N. Hardisty⁽¹⁾, J. P. Moehle⁽²⁾, T. Paret⁽³⁾, S. Pujol⁽⁴⁾

⁽¹⁾ PhD Student, UC, Berkeley, hardisty@berkeley.edu

⁽²⁾ T.Y. and Margaret Lin Professor of Engineering, UC, Berkeley, moehle@berkeley.edu

⁽³⁾ Senior Principal, Wiss, Janney, Elstner Associates, Inc., tparet@wje.com

⁽⁴⁾ Professor of Civil Engineering, Purdue University, spujol@purdue.edu

Abstract

The profession has had very few opportunities to study in detail the response of instrumented buildings subjected to earthquake ground motions that caused severe damage. A case study examines an instrumented building and its response to moderate earthquake ground motion. The building sustained critical damage in a solid wall panel located below a stack of openings between two slab-coupled walls. Performance of the building was studied by examining the measured response, comparing it with response calculated using dynamic analysis, and analyzing demands and capacities of the damaged wall panel zone. The study indicates that geometric and reinforcement discontinuities created vulnerabilities in a structure that, otherwise, should have been expected to survive the ground motion with cosmetic damage only. The study illustrates the importance of paying attention to the effects of discontinuities on the seismic response of structural walls.

Keywords: shear wall; structural discontinuity; damage survey; design recommendations

1. Introduction

An instrumented ten-story building was surveyed in detail after it was damaged by moderate ground motion [$PGV = 14 \text{ in./s}$ (0.35 m/s), $PGA = 0.2g$]. The survey revealed severe damage in slab-coupled structural walls. The structure and the survey results are described, and plausible sources of damage are discussed. Acceleration records obtained near the foundation and near the roof are presented and analyzed. Results of numerical analyses are compared with the measured building response. Recommendations are given to avoid the observed damage.

2. The Building

The building has ten stories above ground (Fig. 1). The floor levels are numbered sequentially from the base to the roof, with the grade level labeled Floor 1. The first story is 24-ft (7.3-m) tall to accommodate a mezzanine, with shorter story heights above the first story. The floor plan, essentially identical at each level, is nearly square with a square central atrium (Fig. 2).

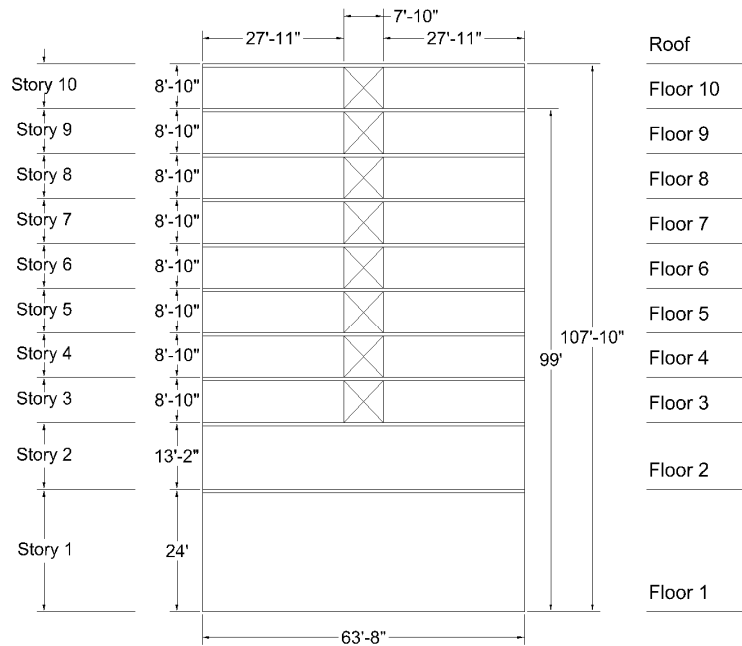


Fig. 1 – Typical wall elevation (Note: 1 in. = 25.4 mm, 1 ft = 305 mm)

The lateral-force-resisting system consists of eight cast-in-place structural walls organized in pairs of orthogonal walls located near each corner of the floor plan (Fig. 2). Each wall consists of two wall piers that are coupled by a reinforced concrete slab from Floors 3 through 10, creating a series of corridor openings (Fig. 1). Below Floor 3, the walls are supported by a common two-story high “podium wall” (Fig. 3), resulting in a solid wall panel beneath the stack of corridor openings. Below Floor 7, the structural walls are 24-in. (0.61-m) thick. Above Floor 7, they are 18-in. (0.46-m) thick. The remainder of the structural system comprises 8-in. (0.20-m) thick unbonded post-tensioned floor slabs supported by 18-in. (0.46-m) square columns (Fig. 2). The building was not perfectly symmetrical, but was assumed so to test the ability of a 2D-model to capture what occurred.

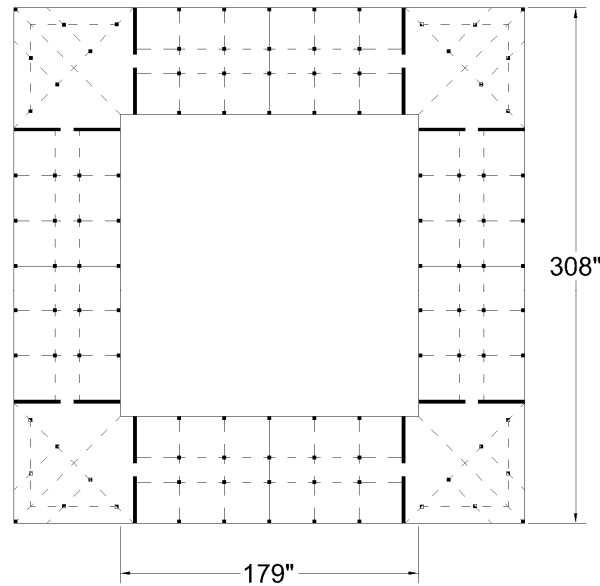


Fig. 2 – Typical floor plan (Note: the details of the building plan have been modified for simplicity, as well as to mask the building identity; 1 ft = 305 mm)

The building is founded on Soil Type E [$V_s < 650$ ft/s (200 m/s)], as classified in [1]. Walls and columns are supported by piles grouped under pile caps. Piles under walls are grouped near each wall end (Fig. 3). Grade beams connect pile caps to one another. The atrium floor is supported grade beams and piles.

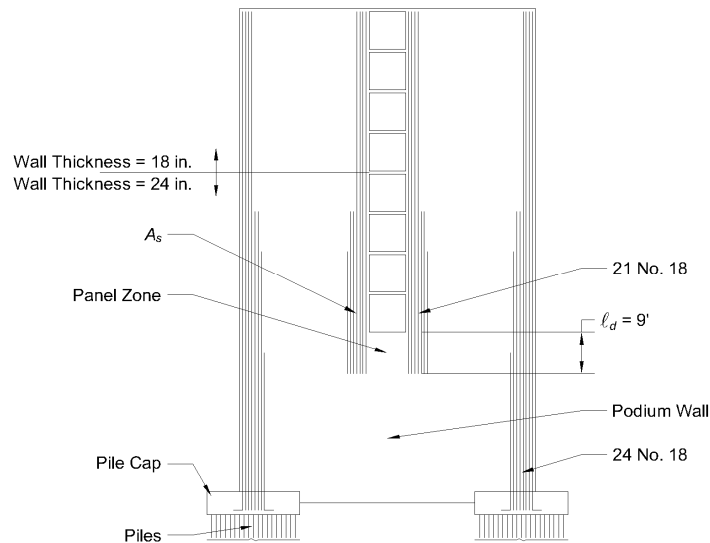


Fig. 3 – Wall elevation and definitions (Note: 1 in. = 25.4 mm, 1 ft = 305 mm)

Concrete cores were extracted after the earthquake. Measured compressive strength varied between samples. The mean value in the zones that were most affected by the ground motion (wall segments in the second story) was 7200 psi (50 MPa), and the standard deviation was 1000 psi (7 MPa).

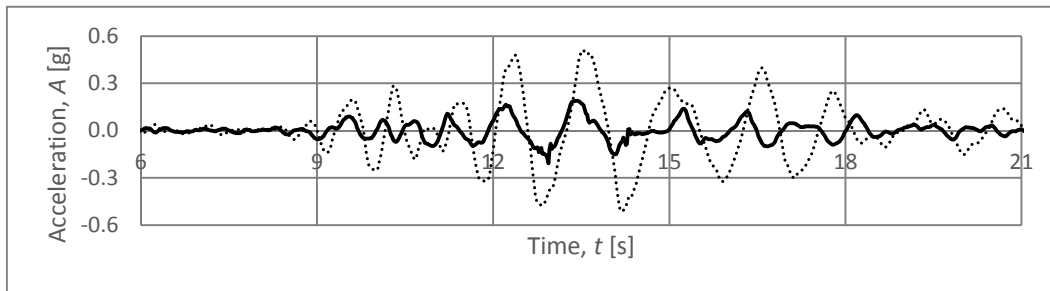
The reinforcement specified in construction drawings is Grade 60 A706 deformed reinforcing bars. In the lower three stories, vertical boundary element reinforcement is 24 and 21 No. 18 (No. 57) bars (Fig. 3). The vertical

reinforcement [21 No. 18 (No. 57) bars] in the boundary elements flanking the hallway openings is terminated 9 ft (2.7 m) into the podium wall. In the lower three stories, the ratio of vertical boundary reinforcement area to the gross area of the boundary element ranges from 7% to 8%. Vertical web reinforcement ratios vary between 0.28% and 0.42%, horizontal web reinforcement ratios vary between 0.42% and 0.83%, and volumetric confining reinforcement ratios vary between 0.8% and 1.2%.

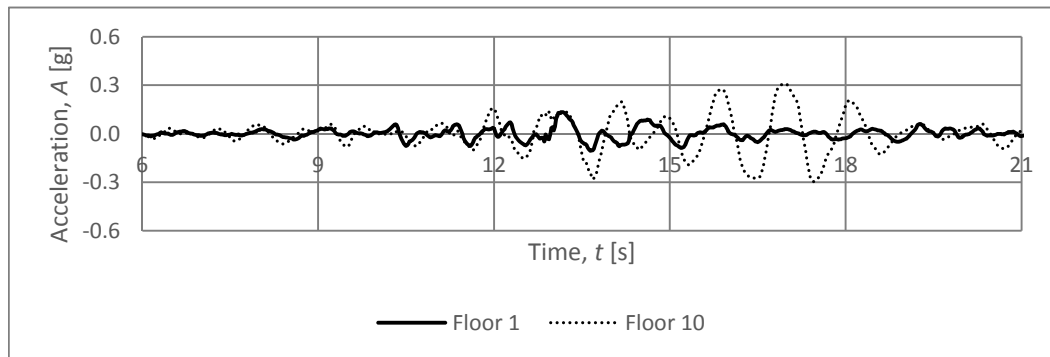
Measured strengths of steel and concrete samples exceeded the values specified in construction drawings. As-built dimensions and reinforcement sizes, quantities, and spacing met what was specified in the original design documents within reasonable tolerances.

3. The Earthquake Records

The moment magnitude of the earthquake was 6.9 and the fault mechanism was oblique with right-lateral strike-slip and reverse-slip components. The epicentral distance was 46.5 mi (74.9 km) and the distance to the closest rupture point was 33.8 mi (54.3 km). Accelerometers recorded motions at Floor 1 (grade level) and Floor 10 (one level below the roof) (Fig. 4). The peak acceleration measured at ground level (*PGA*) was 0.2g in the EW direction and 0.1g in the NS direction. The derived velocity at ground level *PGV* was 14 in./s (0.35 m/s) and 8 in./s (0.2 m/s) in the EW and NS directions, respectively. Fig. 5 shows linear displacement response spectra (for damping coefficients of 2% and 5%) calculated for the more demanding ground motion (EW). For the building site and soil type E, design values from [1] are $SD_5 = 1.25g$ and $SD_1 = 1.6g$. Using the design response spectrum from [1] and defining spectral displacement as spectral acceleration divided by the square of the circular frequency, the 5% damped linear design displacement response spectrum based on [1] is as shown by the dotted curve in Fig. 5. The 5% linear response spectrum for the record obtained at the site is well within the linear design displacement response spectrum, indicating that the recorded ground motion was moderate.



(a) EW



(b) NS

Fig. 4 – Acceleration response records

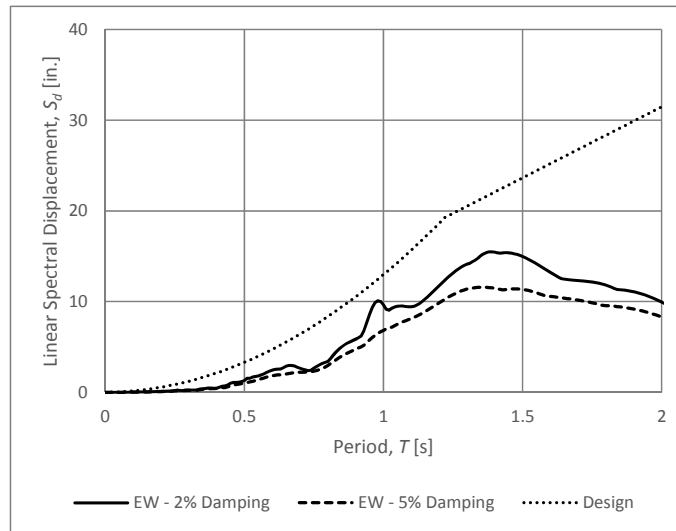


Fig. 5 – Linear displacement response spectra (Note: 1 in. = 25.4 mm)

Floor 10 acceleration records were integrated twice and filtered to remove permanent drifts believed to be associated with instrument error. This was accomplished by excluding frequencies lower than 1/4 Hz in the frequency domain of the acceleration records. Inferred mean drift ratios (differences in displacements at Floor 10 and Floor 1 divided by height from Floor 1 to Floor 10) are shown in Fig. 6. Peak mean drift ratios were approximately 0.8% and 0.4% in the EW and NS directions, respectively.

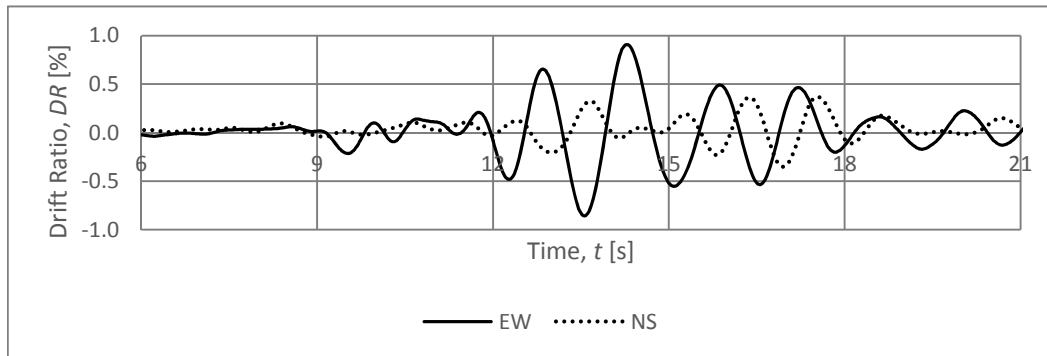


Fig. 6 – Drift ratio response records

According to [2], an upper-bound estimate of roof drift ratio (DR), for a structure that sustains its lateral strength while responding in its nonlinear range through repeated displacement reversals, is given by:

$$DR = \frac{1}{\sqrt{2}} \times T \times PGV \times \Gamma \times \frac{1}{H} \quad (1)$$

where T = first-mode period of the building based on gross sections (calculated as 0.57 s assuming a fixed base and considering wall stiffness only); Γ = modal participation factor (estimated to be 1.5); and H = distance from Floor 1 to the roof [approximately 1300 in. (33 m)].

An alternative method to estimate the roof drift ratio is given by:

$$DR = S_d(T_{cr}) \times \Gamma \times \frac{1}{H} \quad (2)$$

where $S_d(T_{cr})$ = linear spectral displacement at a period of T_{cr} and for a damping ratio of 2%, where T_{cr} is the first-mode period of the building based on cracked sections. This period was taken as $T_{cr} = \sqrt{2}T$.

Eq. (1) yields $DR \approx 0.7\%$ and 0.4% while Eq. (2) yields $DR \approx 0.9\%$ and 0.5% for the EW and NS directions, respectively. These values for roof drift ratio compare well with the peak mean (Floor 10) drift ratios inferred from acceleration records: 0.8% and 0.4% .

The records and the estimated drift ratios show that excitation and response were 1) larger in the EW direction, and 2) not clear indicators of high probability of severe damage.

Fig. 7 plots “inferred (or instantaneous) period,” calculated as twice the interval between consecutive zero crossings in the EW acceleration record from Floor 10. The inferred period shifted from approximately 0.6 to 1.4 s. between 12 and 14 s. This shift indicates that stiffness decreased to approximately 20% of its initial value, suggesting damage occurred between 12 and 14 s.

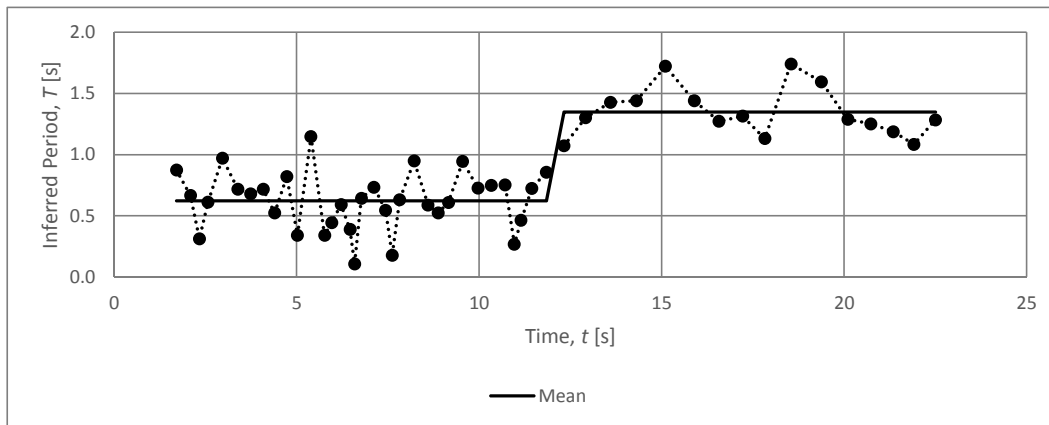


Fig. 7 – Inferred variation of period with time (EW)

The EW ground motion records show three “blips” between 13 and 14 s (Fig. 8). Three blips also appear in the vertical ground acceleration record (Fig. 8). The onset of these blips coincide with times of peak EW acceleration at Floor 10. Coupled with the aforementioned shift in period, it is plausible that the blips were a manifestation of damage or of response of a damaged structure.

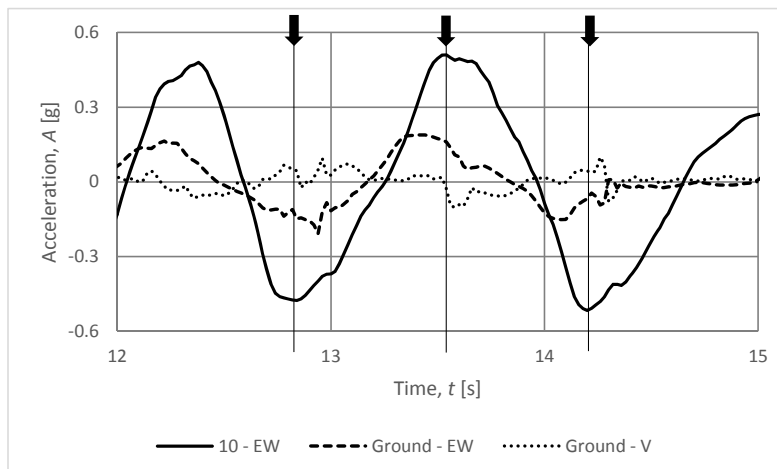


Fig. 8 – “Blips” in acceleration records

4. Damage

Damage surveys were conducted after the earthquake. The greatest concentration of damage was in the podium wall in the region beneath corridor openings (Fig. 9). These regions are referred to as “panel zones” in this paper. Panel zones in walls oriented in the EW direction had more damage than panel zones in walls oriented in the NS direction, which is consistent with the measured differences in excitation and response. EW panel zones had nearly complete disintegration of concrete [Fig. 9(a)], to the extent that a person could see through the walls at several locations. Damage in NS panel zones was limited to cover delamination and inclined cracking [Fig. 9(b)]. The observed damage extended into the boundary elements on either side of the panel zones. In EW walls in which additional wall openings were present under panel zones, damage extended to the foundation. Floor slabs were also damaged where they framed into structural walls. In cases where openings were present below the panel zone, boundary reinforcement extended all the way to the foundation. Earthquake demands caused damage to grade beams at these locations. No damage was observed in inspected piles.

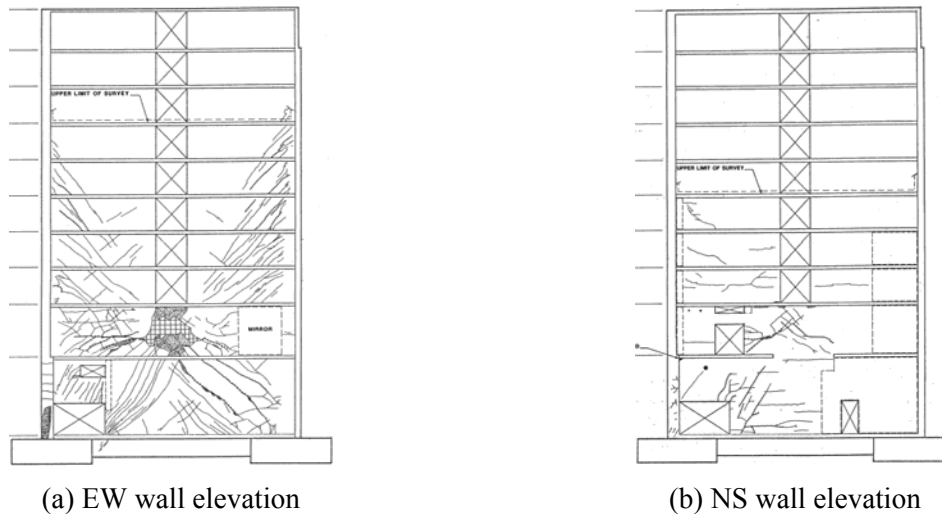


Fig. 9 – Observed damage

5. Preliminary Evaluation of the Wall Panel Zones

Earthquake demands cause alternating tensile and compressive forces in wall boundaries flanking corridors. These forces must be developed in the podium wall beneath. Studies [3], [4], [5], and [6] have concluded that most of the boundary element force is resisted by shear within the panel zone.

In this building, 21 No. 18 (No. 57) Grade 60 A706 boundary element bars flank each side of each corridor opening. These boundary bars terminate 9 ft (2.7 m) into the podium walls. Assuming 100% of the tensile force in a boundary element is resisted by panel zone shear, and assuming the bars develop 1.25 times an expected yield stress of 70 ksi (480 MPa), the panel zone shear can be estimated to be $1.25 \times 70 \text{ ksi} \times 21 \times 4 \text{ in.}^2 = 7,400 \text{ kips}$ (33,000 kN). Distributing this shear uniformly over the height and thickness of the panel zone [as defined by the 9 ft (2.7 m) extent of the boundary bars], the nominal panel zone shear stress is $(7,400 \text{ kips}) / (108 \text{ in.} \times 24 \text{ in.}) = 2.9 \text{ ksi}$ (20 MPa). Considering an average concrete compressive strength of 7200 psi (50 MPa), this corresponds to a nominal shear stress of $33\sqrt{f'_c}$ psi ($2.8\sqrt{f'_c}$ MPa). Damage to the panel zones is not surprising given such large estimated shear stresses.

6. Nonlinear Analysis Model

A 2D numerical model of the building structure was constructed and analyzed in PERFORM-3D [7]. The building was idealized by assuming:



1) reactive mass included self-weight and 25% of the design live load [8], resulting in a mean unit weight of 170 psf (8100 N/m²); 2) wall axial load was proportional to tributary area (approximately 10% of the typical floor area) and includes self-weight, resulting in a ratio of axial force to gross wall area of $0.02f'_c$; 3) foundations were fixed; 4) slabs were rigid in their own planes; 5) slab stiffness could be estimated using the effective width from [9] for slab-wall coupling and [10] for slab-column framing; 6) vertical transient accelerations had negligible effects; 7) there was no reinforcement slip; 8) wall openings – other than corridors – had negligible effects; 9) energy dissipation not related to hysteresis can be represented by Rayleigh damping with 2% of critical damping at 0.9 and 1.1 times the first-mode period calculated using gross sections; and 10) the axial tensile strength of concrete was negligible.

Three models were built: A, B, and C. Model A was linear. Model B used Eq. (3) for concrete in compression [11], Eq. (4) for steel [12], and a linear model for shear. Model C was similar to Model B, but used Eq. (5) for shear [13]. Default values were used to define hysteretic rules.

$$f_c = 0.85f'_c \begin{cases} 2 \frac{\epsilon_c}{\epsilon_o} - \left(\frac{\epsilon_c}{\epsilon_o}\right)^2 & \text{if } \epsilon_c < \epsilon_o \\ 1 - \frac{\epsilon_c - \epsilon_o}{0.01 - \epsilon_o} & \text{otherwise} \end{cases} \quad (3)$$

f_c = concrete stress; f'_c = mean measured concrete core strength [7200 psi (50 MPa)]; ϵ_c = concrete strain; $\epsilon_o = 2(0.85f'_c)/E_c$; E_c = assumed concrete elastic modulus [4800 ksi (33000 MPa)].

$$f_s = \begin{cases} (E_s \epsilon_s \leq f_y) & \text{if } \epsilon_s < \epsilon_{sh} \\ f_{su} + (f_{su} - f_y) \left(\frac{\epsilon_{su} - \epsilon_s}{\epsilon_{su} - \epsilon_{sh}}\right)^P & \text{otherwise} \end{cases} \quad (4)$$

f_s = steel stress; ϵ_s = steel strain; E_s = steel elastic modulus [29000 ksi (200000 MPa)]; f_y = yield stress [70 ksi (480 MPa)]; ϵ_{sh} = strain at the onset of strain hardening (0.016); f_{su} = ultimate stress [95 ksi (660 MPa)]; ϵ_{su} = ultimate strain (0.05); $P = E_{sh}[(\epsilon_{su} - \epsilon_{sh})/(f_{su} - f_y)]$; E_{sh} = strain hardening modulus ($0.05E_s$) [11].

$$v = \begin{cases} 0.4E_c\gamma \leq 3\sqrt{f'_c} + \min(\rho_t, \rho_\ell) f_y \text{ (psi)} \\ 0.25\sqrt{f'_c} + \min(\rho_t, \rho_\ell) f_y \text{ (MPa)} \end{cases} \leq 0.25f'_c \quad (5)$$

v = shear stress; γ = shear strain; ρ_t = transverse reinforcement ratio; ρ_ℓ = longitudinal reinforcement ratio. The shear resistance defined by Eq. (5) was limited to $\gamma \leq 0.01$. For $\gamma > 0.01$, $v = 0$ was assumed based on data reported by [11], [14], [15], and [16]. For the panel zones just below corridors, reinforcement ratios were $\rho_t = 0.0042$ and $\rho_\ell = 0.0028$, resulting in a limiting shear strength $v_u = 450$ psi (3.1 MPa).

Static analyses showed slab-column frames provided less than 10% of the lateral resistance provided by walls. Therefore, their lateral resistance was neglected in dynamic analyses. Walls were discretized into elements of height equal to floor height except where nonlinearity was likely to have occurred (Fig. 10). Wall reinforcement ratios and shear strengths obtained with Eq. (5) are listed in Table 1.

Table 1 – Model summary

Group	ρ_e	ρ_t	v_n	Group	ρ_e	ρ_t	v_n
	(%)	(%)	(ksi)		(%)	(%)	(ksi)
A	0.85	0.27	0.44	G	8.00	0.83	0.54
B	2.26	0.41	0.44	H	0.27	0.27	0.44
C	4.00	0.28	0.45	I	0.27	0.41	0.44
D	6.00	0.28	0.45	J	0.28	0.28	0.45
E	7.00	0.42	0.45	K	0.28	0.42	0.45
F	8.00	0.42	0.54	L	0.42	0.83	0.54

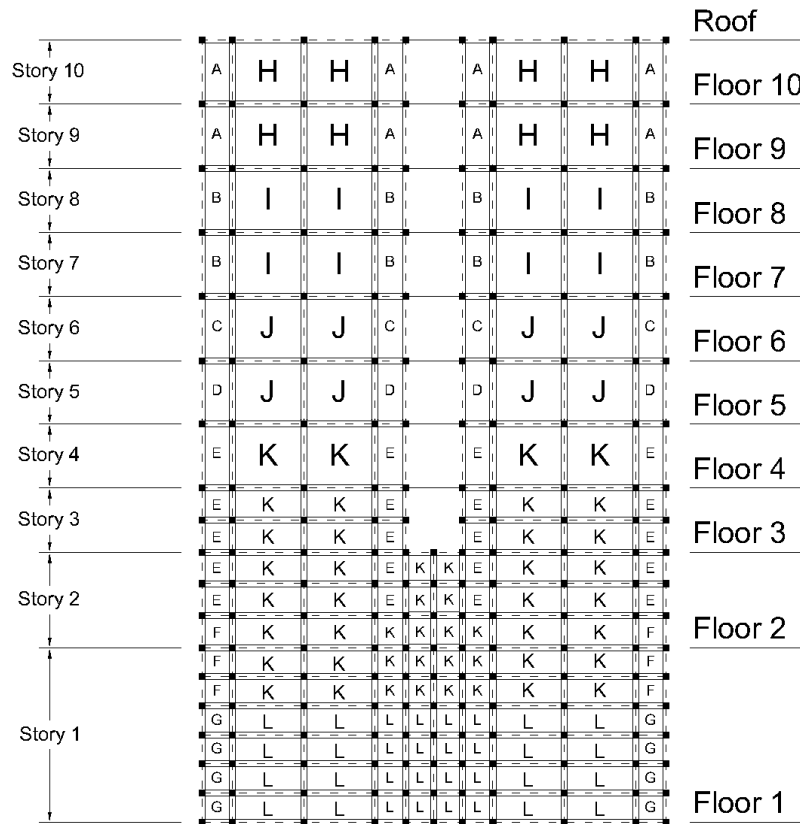


Fig. 10 – Model mesh

The wall model was composed of shear-wall elements native to PERFORM-3D [17]. These elements have 4 nodes, each with 6 degrees of freedom. They are comprised of a shear material and fiber cross section that governs the axial-bending properties of the element. Axial strain, shear strain, and curvature are assumed constant along the element length.

7. Analysis Results

Fig. 11 shows calculated and measured responses in the EW direction. Model A produced a reasonable match up to approximately 13 s, which is close to when a period shift occurred (Fig. 7). Model B did not produce clear improvement. Results from Model C followed the measured acceleration through approximately $t = 14$ s. Beyond $t = 12$ s, it is plausible that damage caused torsion and strengthened the existing asymmetry not captured by the models.

For Model C, calculated shear deformations were largest in the panel zone (between the development lengths of contiguous boundary reinforcement). Panel zone shear stress in this region reached the strength obtained from Eq. (5) at $t = 9.5$ s. Calculated shear strains reached the assumed “limit” strain of 0.01 at $t = 12$ s. For $t > 12$ s, the maximum average shear strain in the panel zone was 0.022.

Fig. 12 plots the measured and calculated responses (for Model C) in the NS direction. Amplitudes are similar through $t = 12$ s (the inferred time of damage onset), but waveforms do not match as well as for the EW direction. For NS, panel-zone peak calculated shear strains reached 0.4% (1/6 the peak strain for EW). Shear stresses also reached the capacity estimated with Eq. (5).

The models were also used to explore the effect of extending the boundary element longitudinal reinforcement all the way to foundation level, rather than terminating it at $\ell_d = 9$ ft (2.7 m) into the podium wall.

Analyses of a variant of Model B in which tension reinforcement flanking the panel zone was assumed to be anchored into the foundation showed that, if the panel zone remains linear in shear, the region within ℓ_d from the lowest opening can attract as much as 70% of the force in the boundary reinforcement flanking it.

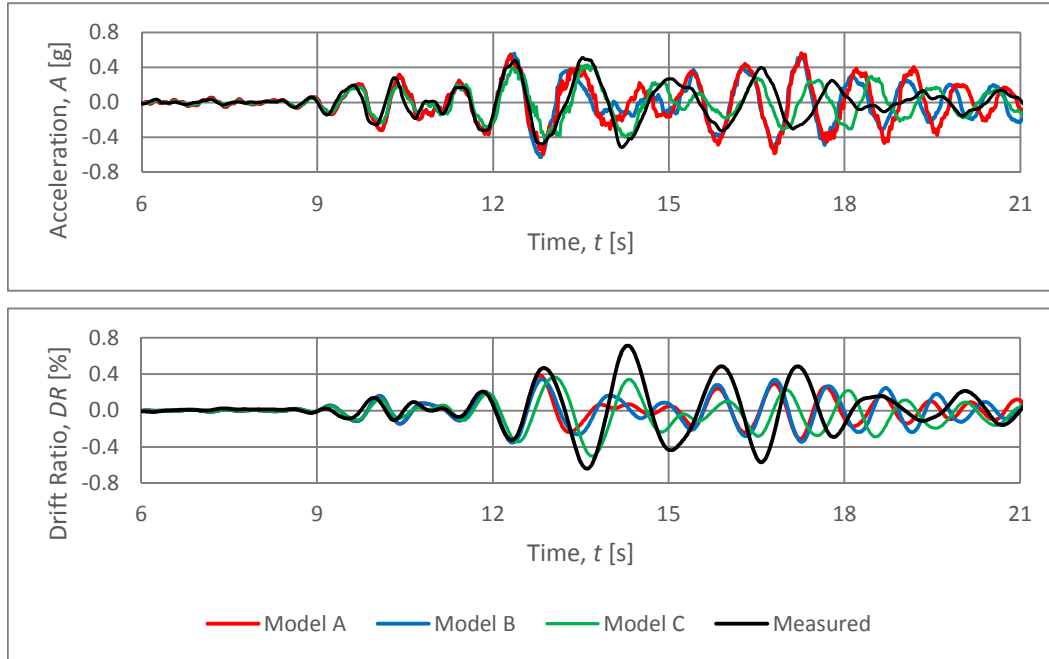


Fig. 11 – Calculated and measured Floor 10 responses (EW)

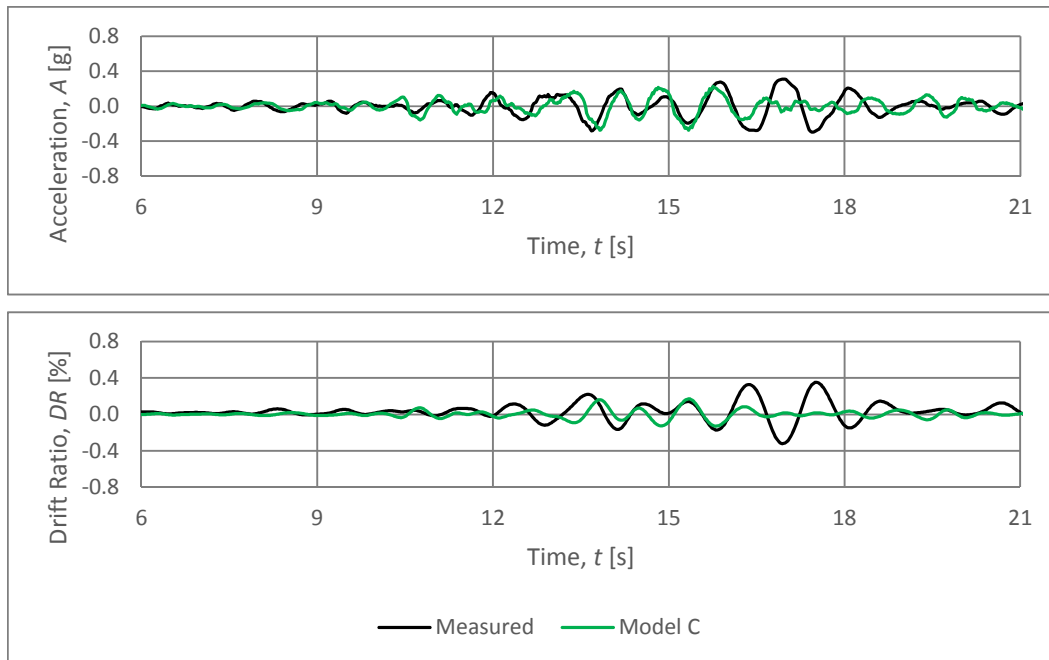


Fig. 12 – Computed and measured Floor 10 responses (NS)



Analyses of a variant of Model C in which 1) tension reinforcement flanking the panel zone is assumed to be anchored into the foundation, and 2) the panel zone is assumed to have bilinear response to shear [Eq. (5)], showed that the additional anchorage may help control shear deformations in the panel zone.

8. Summary and Conclusions

Moderate earthquake ground motion caused severe damage to structural walls in an instrumented ten-story building. The walls were separated by corridor openings in stories 3 through 10, and were supported on solid podium walls in stories 1 and 2. Longitudinal reinforcement in boundary elements flanking corridors terminated one development length ℓ_d into the podium wall. For EW walls, the wall panel beneath corridors was severely damaged, with damage extending along the development length of the curtailed boundary element bars. The damage highlights a common design problem – using the development length specified for one bar as the length for a large number of bars can result in overloading the concrete, causing local failure not expected for a single bar.

Assuming that the tensile force in the curtailed longitudinal bars had to be resisted by the wall panel zone between the curtailed bars led to estimated shear stresses well beyond the capacity of lightly reinforced concrete. Nonlinear dynamic analyses also indicated that panel zone beneath corridors would have reached 1) its shear strength and 2) for EW walls, shear strains exceeding reasonable limits.

The evidence discussed suggests that the panel zone (wall segment under corridors) should be detailed to resist a unit shear stress approaching:

$$v_u = \frac{T}{b_w \times h_w} \quad (6)$$

where v_u = unit shear stress; h_w = height of panel zone; b_w = thickness; $T = 1.25 \times A_s \times f_y$; A_s = area of boundary element steel flanking panel zone. Boundary element reinforcement anchorage length should exceed h_w . h_w should be selected to make v_u smaller than the limits of Eq. (5).

9. Acknowledgements

The authors would like to thank Computers and Structures, Inc. for their generous donation of PERFORM-3D, which was used to perform the analyses in this study.

10. References

- [1] ASCE 7-10 (2010), “Minimum Design Loads for Buildings and Other Structures,” American Society of Civil Engineers, May, 650 pp.
- [2] Sozen, M. A. (2003), “The Velocity of Displacement,” *Proceedings of the NATO Science for Peace Workshop on Seismic Assessment and Rehabilitation of Existing Buildings*, May, pp. 11-28.
- [3] Naeim, F.; Schindler, B.; Martin, J. A., Jr.; and Lynch, S. (1990), “Hidden Zones of High Stress in Seismic Response of Structural Walls,” *Proceedings of the SEAOC Annual Convention*, Sept., pp. 402-422.
- [4] NIST (2014), “Recommendations for Seismic Design of Reinforced Concrete Wall Buildings Based on Studies of the 2010 Maule, Chile Earthquake,” *NIST GCR 14-917-25*, National Institute of Standards and Technology, Mar., 290 pp.
- [5] Villalobos, E. J. (2014), “Seismic Response of Structural Walls with Reinforcement and Geometric Discontinuities,” *PhD Thesis*, Lyles School of Civil Engineering, Purdue University, Aug., 334 pp.
- [6] Moehle, J. (2014), “Seismic Design of Reinforced Concrete Buildings,” McGraw-Hill, New York, Oct., 592 pp.
- [7] CSI (2011), “PERFORM-3D: Nonlinear Analysis and Performance Assessment for 3-D Structures,” Version 5, Computers and Structures, Inc., Jun.
- [8] PEER/ATC (2010), “Modeling and acceptance criteria for seismic design and analysis of tall buildings,” *No. PEER/ATC 72-1*, Applied Technology Council, Oct., 242 pp.



- [9] Schwaighofer, J., and Collins, M. P. (1977), "Experimental Study of the Behavior of Reinforced Concrete Coupling Slabs," *ACI Journal*, V. 74, No. 3, Mar., pp. 123-127.
- [10] Hwang, S.-J., and Moehle, J. P. (2000), "Models for Laterally Loaded Slab-Column Frames," *ACI Structural Journal*, Vol. 97, No. 2, Mar., pp. 345-353.
- [11] Hognestad, E. (1951), "A Study of Combined Bending and Axial Load in Reinforced Concrete Members," V. 49, No. 22, University of Illinois Engineering Experiment Station, University of Illinois at Urbana-Champaign, Nov., 128 pp.
- [12] Mander, J. B.; Priestly, M. J. N.; and Park, R. (1984), "Seismic Design of Bridge Piers," No. 84-02, Department of Civil Engineering, University of Canterbury, Feb., 442 pp.
- [13] Pujol, S. (2014), "Panel Zones in Structural Walls," *UCB SEMM Seminar*, Department of Civil and Environmental Engineering, University of California at Berkeley, Apr.
- [14] Bentz, E. C; Vecchio, F. J.; and Collins, M. P. (2006), "Simplified Modified Compression Field Theory for Calculating Shear Strength of Reinforced Concrete Elements," *ACI Structural Journal*, V. 103, No. 4, July-Aug., pp. 614-624.
- [15] Mansour, M., and Hsu, T. T. C. (2005), "Behavior of Reinforced Concrete Elements under Cyclic Shear. I: Experiments," *Journal of Structural Engineering*, Vol. 131, No. 1, Jan., pp. 44-53.
- [16] Vecchio, F. J., and Collins, M. P. (1981), "Stress-strain characteristics of reinforced concrete in pure shear," *IABSE Colloquium*, June, pp. 212-225.
- [17] CSI (2011), "Components and Elements for PERFORM-3D and PERFORM-COLLAPSE," Version 5, Computers and Structures, Inc., Jun., pp. 120-130.
- [18] Bournonville, M., Dahnke, J.; and Darwin, D. (2004), "Statistical Analysis of the Mechanical Properties and Weight of Reinforcing Bars," *SL Report, No. 04-1*, Structural Engineering and Materials Laboratory, The University of Kansas, Dec., 198 pp.
- [19] Hall, J. F. (2006), "Problems encountered from the use (or misuse) of Rayleigh damping," *Earthquake Engineering and Structural Dynamics*, V. 35, No. 5, Apr., pp. 525-545.
- [20] Mansour, M., and Hsu, T. T. C. (2005), "Behavior of Reinforced Concrete Elements under Cyclic Shear. II: Theoretical Model," *Journal of Structural Engineering*, Vol. 131, No. 1, Jan., pp. 54-65.
- [21] Pang, X. B., and Hsu, T. T. C. (1995), "Behavior of Reinforced Concrete Membrane Elements in Shear," *ACI Structural Journal*, V. 92, No. 6, Nov.-Dec., pp. 665-677.
- [22] Stevens, N. J.; Uzumeri, S. M.; and Collins, M. P. (1991), "Reinforced Concrete Subjected to Reversed Cyclic Shear – Experiments and Constitutive Model," *ACI Structural Journal*, V. 88, No. 2, Mar.-Apr., pp. 135-146.
- [23] Tanyeri, A. C., and Moehle, J. P. (2014), "Collapse of a Concrete Wall Building in the 2010 Chile Earthquake," *No. UCB/SEMM-14/02*, Mar., 35 pp.
- [24] Vecchio, F. J., and Collins, M. P. (1986), "The Modified Compression-Field Theory for Reinforced Concrete Elements Subjected to Shear," *ACI Journal*, V. 83, No. 2, Mar.-Apr., pp. 219-231.